⌘ *Author's Choice*

THE JOURNAL OF BIOLOGICAL CHEMISTRY VOL. 287, NO. 23, pp. 19115–19121, June 1, 2012

Mutation of Conserved Histidines Alters Tertiary Structure and Nanomechanics of Consensus Ankyrin Repeats*[S]

Received for publication, March 23, 2012 Published, JBC Papers in Press, April 18, 2012, DOI 10.1074/jbc.M112.365569

Whasil Lee[‡], Johan Strümpfer[§], Vann Bennett[¶1], Klaus Schulten[§2], and Piotr E. Marszalek[‡3]

From the [‡]Center for Biologically Inspired Materials and Material Systems and Department of Mechanical Engineering and Materials Science and the [¶]Howard Hughes Medical Institute and Department of Cell Biology, Duke University, Durham, North Carolina 27708 and the [§]Center for Biophysics and Computational Biology and Beckman Institute, University of Illinois at Urbana-Champaign, Urbana, Illinois 61801

Background: The His → Arg mutation in a native ankyrin-R protein is responsible for converting RBCs to spherocytes, causing hereditary spherocytosis (HS).
Results: The mutant unfolds and refolds at lower forces compared with the wild type.
Conclusion: The His → Arg mutation weakens the mechanical stability of ankyrin repeats.
Significance: The His → Arg mutation in ankyrin-R may cause HS by decreasing the mechanical stability and affecting its structure recovery ability.

The conserved TPLH tetrapeptide motif of ankyrin repeats (ARs) plays an important role in stabilizing AR proteins, and histidine (TPLH)-to-arginine (TPLR) mutations in this motif have been associated with a hereditary human anemia, spherocytosis. Here, we used a combination of atomic force microscopy-based single-molecule force spectroscopy and molecular dynamics simulations to examine the mechanical effects of His → Arg substitutions in TPLH motifs in a model AR protein, NI6C. Our molecular dynamics results show that the mutant protein is less mechanically stable than the WT protein. Our atomic force microscopy results indicate that the mechanical energy input necessary to fully unfold the mutant protein is only half of that necessary to unfold the WT protein (53 *versus* 106 kcal/mol). In addition, the ability of the mutant to generate refolding forces is also reduced. Moreover, the mutant protein subjected to cyclic stretch-relax measurements displays mechanical fatigue, which is absent in the WT protein. Taken together, these results indicate that the His → Arg substitutions in TPLH motifs compromise mechanical properties of ARs and suggest that the origin of hereditary spherocytosis may be related to mechanical failure of ARs.

Ankyrin repeats (ARs)[4] are one of the most common motifs of repeat proteins with a high degree of amino acid sequence homology. ARs fold into nearly identical helix 1-helix 2-loop structures and stack to form elongated superhelical domains that frequently mediate protein-protein interactions (1–3). Previously, single-molecule force spectroscopy experiments of a few AR proteins revealed that mechanically unfolded ARs refold rapidly and generate very robust refolding forces (4–9). Recently, we examined in detail the mechanical properties of a model synthetic AR protein, NI6C (7). NI6C is composed of six identical internal ARs based on a consensus sequence and two capping repeats (10). Our atomic force microscopy (AFM) manipulations on NI6C presented very interesting mechanical properties. We observed that NI6C unfolds stepwise, repeat by repeat, and individual unfolding events produce regular, well resolved force peaks of ~22 piconewtons (pN). In addition, relaxation traces of NI6C captured robust refolding force peaks and revealed no elastic hysteresis or fatigue, suggesting that this protein possesses superior elastic properties (7).

It has been suggested that the conserved TPLH tetrapeptide motif of ARs plays an important role in stabilizing AR proteins (2, 11–13). Some mutations in the TPLH motif, including Thr → Ala, His → A, and/or His → Gln substitution, were found to significantly affect the thermal stability of gankyrin (11). However, the role of the TPLH motif in the mechanical stability of ARs has not been studied.

Hereditary spherocytosis (HS) is a life-threatening human anemia in which erythrocytes (RBCs) lose their characteristic shape and become spherical and very fragile (14, 15). HS is caused by defects in proteins that mediate membrane-cytoskeleton connections in erythrocytes such as ankyrin-R, spectrins, and band 3 (1, 14, 16). There are two missense mutations identified so far in the AR segment of ankyrin-R that are related to HS: H277R and V463I (14, 16). Importantly, the His → Arg substitution involves a highly conserved histidine of the TPLH motif.

Because RBCs undergo repeated cycles of stress and deformation while flowing through narrow capillaries and slits of the spleen (16, 17), the elastic response of the membrane and associated cytoskeletal proteins to the applied forces is essential for

* This work was supported, in whole or in part, by National Institutes of Health Grants GM079663 (to P. E. M. and V. B.) and P41-RR005969 and R01-GM073655 (to J. S. and K. S.).
⌘ *Author's Choice*—Final version full access.
[S] This article contains supplemental Figs. S1–S3 and Table S1.
[1] Howard Hughes Medical Institute Investigator. To whom correspondence may be addressed: Duke University, 361 CARL Bldg., Durham, NC 27710. Fax: 919-684-3590; E-mail: benne012@mc.duke.edu.
[2] To whom correspondence may be addressed: 3147 Beckman Institute, Urbana, IL 61801. Fax: 217-244-6078; E-mail: kschulte@ks.uiuc.edu.
[3] To whom correspondence may be addressed: Duke University, 144 Hudson Hall, Durham, NC 27708. Fax: 919-660-8963; E-mail: piotr.marszalek@duke.edu.
[4] The abbreviations used are: AR, ankyrin repeat; AFM, atomic force microscopy; N, newton(s); HS, hereditary spherocytosis; MD, molecular dynamics; SMD, steered MD; r.m.s., root mean square.

maintenance of RBC integrity and to enable recovery. Force-induced unfolding of spectrin was already captured in live RBCs under physiological stress (18). It is therefore possible that ankyrin-R, depending on the (presently unknown) direction and magnitude of applied forces, also undergoes stretch-relax cycles *in vivo*, which may involve all or some of its ARs.

The goal of this work was to test the hypothesis that His → Arg substitutions in the TPLH motif disrupt stabilizing interactions and compromise mechanical properties of ARs. Because the membrane-binding domain of ankyrin-R is very large and its crystal structure is not yet available, we decided to carry out our initial studies of the mechanical effect of His → Arg substitution in the TPLH motif in NI6C, which proved to be an excellent model AR system amenable to single-molecule force spectroscopy by AFM (7). To amplify the possible effect of the His → Arg mutation, we substituted TPLH histidines in four internal ARs within NI6C (see Fig. 1*B*). We used a combination of AFM-based single-molecule force spectroscopy (19–27) and molecular dynamics (MD) simulations (9, 28–34) to examine how mutations in this motif affect the mechanical and structural properties of NI6C when the proteins are pulled by their N and C termini. We found that for the particular pulling geometry used in this study (stretching by the N and C termini), the mechanical unfolding forces of the mutant were significantly reduced, and as a result, the total consumed mechanical energy during the unfolding process decreased by half (53 *versus* 106 kcal/mol) compared with WT NI6C, suggesting that His → Arg substitutions indeed alter the mechanical properties of ARs. Furthermore, we registered that the mechanical refolding forces of the mutant were significantly reduced and observed the mechanical fatigue of the mutant over cyclic stretch-relax experiments. Taken together, these observations suggest that the H277R mutation possibly reduces the mechanical robustness of ankyrin-R and may ultimately cause its mechanical failure, leading to HS.

MATERIALS AND METHODS

Cloning, Expression, and Purification of Repeat Proteins—The gene of the mutant protein $NI(I_{H7R})_4IC$ was synthesized by GenScript (Piscataway, NJ). In the mutant protein, four internal consensus ARs (repeats 2–5) were modified by substituting the histidines at position 7 with arginines (see Fig. 1*B*). Please note that in Fig. 1*B*, the TPLH histidines are in position 9. However, this position corresponds to position 7 within the AR sequence according to the residue numbering scheme of ARs introduced by Michaely *et al.* (2). The $NI(I_{H7R})_4IC$ gene was inserted into the poly-I27 pRSETa vector (a kind gift from Jane Clarke; Ref. 35) using KpnI and NheI restriction sites, and the eighth I27 module was replaced with Strep-tag and a stop codon. The engineered plasmids were transformed into *Escherichia coli* C41(DE3) and expressed using isopropyl β-D-thiogalactopyranoside induction. The expressed proteins were purified using a nickel affinity column (GE Healthcare 17-5248-01) followed by a Strep-tag column (IBA 2-1202-0250). Proteins were determined to be >95% pure by SDS-PAGE analysis. The purified proteins were then dialyzed in 150 mM NaCl, 1 mM EDTA, 2 mM tris(2-carboxyethyl)phosphine (Thermo Scientific 77720), and 10 mM Tris buffer (pH 7.4). The final concentration of the purified protein was ~0.3 mg/ml.

AFM-based Single-molecule Force Spectroscopy—All AFM measurements were carried out on custom-built AFM instruments (20, 36, 37) equipped with an AFM detector head (Veeco) and high-resolution piezoelectric stages (Physik Instrumente GmbH), equipped with capacitive or strain gauge position sensors (vertical resolution of 0.1 nm). The spring constant (k_c) of each cantilever was calibrated in solution using the energy equipartition theorem as described (38). All force-extension measurements were performed in solution using BioLever AFM cantilevers (Veeco; $k_c \approx 6$ pN/nm) at pulling speeds of 0.03~0.1 nm/ms at room temperature. Stock protein solutions were diluted to 1~10 μg/ml using 150 mM NaCl, 1 mM EDTA, 2 mM tris(2-carboxyethyl)phosphine, and 10 mM Tris buffer (pH 7.4). 50 μl of the diluted solution was deposited on clean glass substrate, gently washed after 30 min of incubation, and used for AFM pulling experiments.

Single-hit Approach—For AFM-based force spectroscopy measurements, proteins were picked up with an AFM tip by gently contacting the sample substrate at forces <1 nN. Typically, the nonspecific adsorption of proteins to the AFM tip requires multiple attempts to be carried out on the same location before a successful event occurs. However, this approach may result in the mechanical denaturing of proteins. To avoid possible protein damage, we modified this protocol and performed single measurements at a given location, which we call "single-hit approach." If the first attempt was not successful, the AFM tip was moved to a different location for another attempt to pick up a molecule until a successful event occurred. The six I27 domains of titin flanking NI6C and $NI(I_{H7R})_4IC$ proteins (three on each of the N- and C-terminal sides of ARs) served as pulling handles and as a force spectroscopy reference for identifying single-molecule recordings. To establish a mechanical fingerprint of ARs, we fully stretched constructs (extensions of ~400 nm) and selected unfolding force-extension curves with more than four characteristic I27 force peaks (~200 pN, ~28 nm) for single-molecule identification. We used these recordings as the reference force spectrogram to identify unfolding events of ARs in other measurements.

Cyclic Measurements—In some experiments, after a molecule was picked up by using the single-hit approach, we performed cyclic stretch-relax measurements on it. In these measurements, the extension was limited so that I27 domains were not unfolded, and the AFM tip was slightly lifted above the sample substrate (5~10 nm) to prevent adsorption of other molecules.

Mechanical Unfolding Energy Analysis—The WT NI6C protein contains eight ARs: six identical consensus repeats flanked by slightly different N- and C-terminal capping repeats (see Fig. 2) (7). WT ARs unfold sequentially, generating five to six almost uniform unfolding force peaks of ~23 pN, spaced by ~11 nm. Supported by MD simulations, these sharp and regular five to six unfolding force peaks are interpreted to report the unfolding of six internal consensus repeats. The unfolding of the capping repeats is typically unresolved. Because ARs unfold sequentially and we mutated only the internal four repeats, we expect that that the middle peaks in force-extension curves of the mutant

(see Fig. 2*C*) are generated when the mutated internal repeats are unraveled. Often the unfolding force peaks of the mutant were not sharp but smeared and merged, producing a force curve with a shape of a force plateau. For these reasons, it was rather difficult to determine the individual unfolding force peaks and their amplitudes. To quantify mechanically the effect of the mutation, the consumed energy during the unfolding process was calculated for each curve (WT and mutant). As an estimate of this energy input, the area enclosed by the unfolding force-extension curve of ARs (corresponding to the extension between 18 and 81 nm) and the worm-like chain curve drawn through the first I27 unfolding peak was calculated (*yellow* area in supplemental Fig. S2, *C* and *D*). The average "mechanical unfolding energy" defined this way was 53.2 ± 10.9 kcal/mol ($n = 50$) for the mutant and 106.5 ± 12.7 kcal/mol ($n = 12$) for the WT protein. Thus, the four internal AR His → Arg mutations cause the mechanical unfolding work input to decrease by ~50% compared with the WT protein.

MD Simulations—The initial geometry of NI6C (253 amino acids) (7) was built based on Protein Data Bank structure 2QYJ, corresponding to the NI3C consensus AR protein (10). In NI6C, the two capping and all internal repeat amino acid sequences are the same as in NI3C, and only the number of internal repeats is increased in NI6C from three to six. Structure building details have been described (7). The histidines of four internal repeats of NI6C (see Fig. 1*B*) were mutated to arginines using the program VMD (39). Equilibrium MD simulations of both NI6C and the mutant NI(I_{H7R})$_4$IC structures in periodic water boxes ($110 \times 100 \times 100$ Å^3) with 150 mM NaCl, using the CHARMM22 force field (43, 49), were performed with NAMD (40). The force response of each structure was subsequently probed by steered MD (SMD) simulations (41), where the C-terminal C^α of the protein is pulled with a constant velocity (v; by an attached spring force) while the N-terminal C^α is held fixed. Each structure was extended by 50 nm using a pulling velocity of $v = 5$ Å/ns and a spring constant of $3\ k_BT$/Å^2. Simulations were carried out at 310 K and at 1 atm. supplemental Table S1 presents a summary of all simulations performed.

RESULTS AND DISCUSSION

Fig. 1*A* shows a ribbon diagram of the TPLH region in the WT NI6C protein (7, 42). The TPLH motifs are located between the hydrophobic helical bundles and the solvent-exposed loop regions (2). The histidines in the TPLH motifs are located at the beginning of helix 1. As marked by *dotted lines* in Fig. 1*A*, histidines at position 7 and tyrosines at position 4 in TPLH motifs form an H-bond network. Each TPLH histidine forms three H-bonds with the TPLH tyrosine within the same repeat and one H-bond with the TPLH tyrosine of the next AR. The intra-repeat H-bonds are Thr-4 H^N–His-7 $N^{\delta1}$, Thr-4 $O^{\gamma1}$–His-7 H^N, and Thr-4 $H^{\gamma1}$–His-7 $N^{\delta1}$. The inter-repeat H-bond is between His-7 $H^{\epsilon2}$ and Thr-4 O of the next repeat. Because of these extensive interactions, the conserved TPLH motif is vital to the protein structure and its stability (11). For these reasons, we anticipate that His → Arg substitutions in the TPLH motif will likely affect both the structure and stability of AR polypeptides.

Equilibrium Structures of NI6C and NI(I_{H7R})$_4$IC—First we employed MD simulations to test whether the structure of NI6C changes from the His → Arg mutations. Four internal consensus ARs (repeats 2–5) (Fig. 1*B*) of WT NI6C (7) were modified in the NI(I_{H7R})$_4$IC mutant by mutating histidines at position 7 to arginines. Equilibrium all-atom MD simulations of both NI6C and NI(I_{H7R})$_4$IC were performed, totaling 200 ns (see supplemental Table S1 for details). The WT NI6C protein showed little deviation from the initial structures in the equilibrium simulations, with average backbone root mean square (r.m.s.) deviations (C^α r.m.s. deviations) of 1.14, 1.14, and 1.33 Å in each NI6C simulation (Fig. 1*C*). The NI(I_{H7R})$_4$IC mutant showed significantly more deviation from the initial structure, with average C^α r.m.s. deviations of 1.8, 2.1, and 2.2 Å in each simulation. Much of the deviation occurred in the loop regions between the repeats, with an extension of the overall structure from an average length of 73.5 Å for NI6C to 76.2 Å for NI(I_{H7R})$_4$IC. Significant rearrangement of H-bonding in the TPLH motifs occurs due to the His → Arg mutation: the bulkier arginine displaces the inter-AR loop and forms a single H-bond with the aspartic acid in position 32 (in the loop region between ARs), thus altering the average loop orientation with respect to the AR α-helices (Fig. 1*D*). The reduction from three H-bonds, made by the histidine in NI6C, to only one by the arginine in NI(I_{H7R})$_4$IC results in a destabilization of the mutant structure, especially the loop regions, as shown by the r.m.s. fluctuations calculated from the equilibrium MD trajectories (Fig. 1*E*).

In Silico Force Unfolding of NI6C and NI(I_{H7R})$_4$IC—Following equilibrium simulation, we performed two SMD simulations for each NI6C and NI(I_{H7R})$_4$IC, pulling on the C-terminal C^α using a pulling velocity of $v = 5$ Å/ns. The resulting force-extension curves from the simulations are shown in supplemental Fig. S1*A*. The force-extension curves show as much difference between the WT and mutant structures as between repeated SMD simulations of the same structure. All simulations showed major force-rupture peaks spaced every 10 nm, which corresponded to the rupture of each AR. Unfolding of each AR occurred for both the WT and mutant proteins from the C terminus to the N terminus, as reported previously (7). We note, however, that the unfolding pathways as determined through SMD simulations may differ from the pathways explored by the proteins in AFM unfolding measurements, and these issues have to be further examined in future studies. Visual analysis of the SMD simulations showed that the major force-rupture peaks are due to the dissociation of the intra-repeat helices (supplemental Fig. S1*B*). Given the amplitude of fluctuations seen in equilibrium simulations (Fig. 1*E*), slower pulling velocities than those achievable with current computational resources are likely required to capture the mechanistic differences between the force unfolding of NI6C and NI(I_{H7R})$_4$IC.

Mechanical Unfolding of NI(I_{H7R})$_4$IC—To examine the mechanical unfolding behavior of an intact NI(I_{H7R})$_4$IC mutant, we performed single-hit stretching measurements on NI(I_{H7R})$_4$IC-I27 constructs, which were designed to limit possible mechanical damage to the protein resulting from multiple attempts to pick it up by an AFM tip (see "Materials and Methods"). To ease single-molecule force spectroscopy

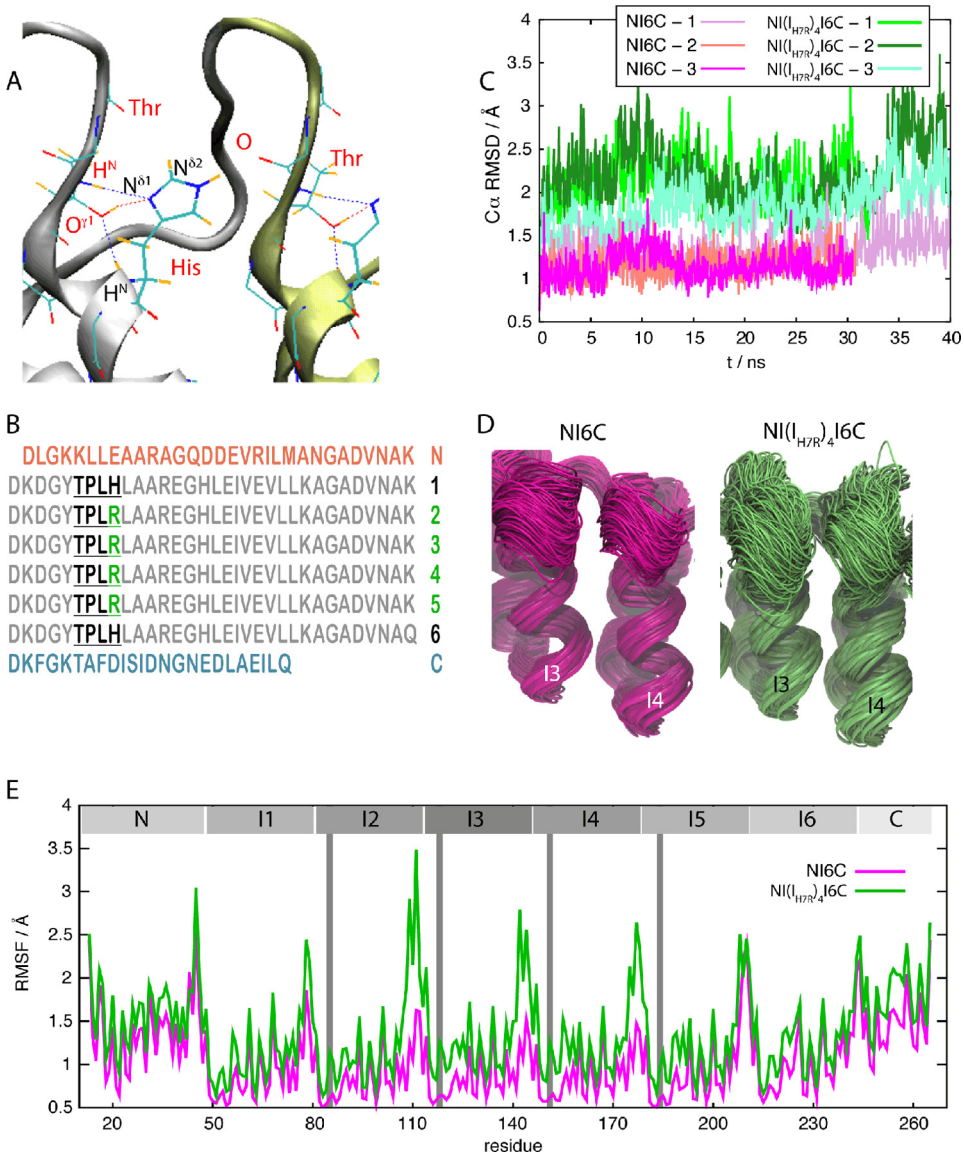

FIGURE 1. **Structures of WT NI6C and mutant $NI(I_{H7R})_4IC$.** *A*, putative H-bonds of a histidine in the TPLH motif in NI6C. These structures were determined based on Refs. 7 and 42. The program MolProbity was used to add hydrogen atoms to the structure with the Asn/Gln/His flip-optimization option on (46–48). Intra- and inter-repeat H-bonds between histidine and tyrosine are depicted by *dotted lines*. *B*, amino acid sequence of $NI(I_{H7R})_4IC$. Histidines of four internal repeats were mutated to arginines using VMD (39). *C*, r.m.s. deviation (*RMSD*) from the initial structure in the simulations, with the WT protein shown in shades of *pink* and the mutant in shades of *green*. *D*, ribbon diagram showing every 200 ps of the equilibrium MD trajectories for internal repeats 3 and 4 (totaling 100 ns for each wild-type and mutant protein). *E*, r.m.s. fluctuations (*RMSF*) averaged over all trajectories for the wild-type (*pink*) and mutant (*green*) equilibrium MD simulations. *Vertical gray bars* indicate the position of the H7R mutation.

measurements and their interpretations, the mutant protein $NI(I_{H7R})_4IC$, similar to the NI6C protein (7), was flanked on each side by three I27 domains of titin, serving as pulling handles and as a force spectroscopy reference for identifying single-molecule recordings (8, 24, 35, 44, 45). Fig. 2*A* (*inset*) shows schematic ribbon diagrams of the chimeric proteins $(I27)_3$-NI6C-$(I27)_3$ and $(I27)_3$-$NI(I_{H7R})_4IC$-$(I27)_3$, which were examined by AFM. Since we studied the mechanical property of WT NI6C previously (7), we compared the AFM results of $NI(I_{H7R})_4IC$ with the force spectra of NI6C. In Fig. 2*A*, we show the representative unfolding force-extension traces that were recorded in single-molecule AFM measurements of NI6C-I27 and $NI(I_{H7R})_4IC$-I27 constructs. Both curves were obtained at the same pulling speed of 0.1 nm/ms. The five I27 unfolding force peaks at extensions above 100 nm provide direct evidence that the whole measurement was obtained on a single molecule containing all eight ARs. Small unfolding force peaks at protein extensions below 100 nm in the *red* and *green curves* strongly suggest that they correspond to the sequential unfolding of NI6C and $NI(I_{H7R})_4IC$, respectively. We used these recordings as the reference force spectra to identify unfolding events of ARs in other measurements on the WT and mutant proteins.

In supplemental Fig. S2 (*A* and *B*), we superimposed AFM recordings of different molecules of the mutant and WT proteins, respectively. In Fig. 2*C*, we compare the AFM recordings of the mutant with a typical unfolding force-extension curve of WT NI6C (7). It is clear that the force-extension curves of the mutant overlap reasonably well with the force-extension curve of WT NI6C at the beginning and at the end. However, at the intermediate extensions (indicated by the *green bar* in Fig. 2*C*),

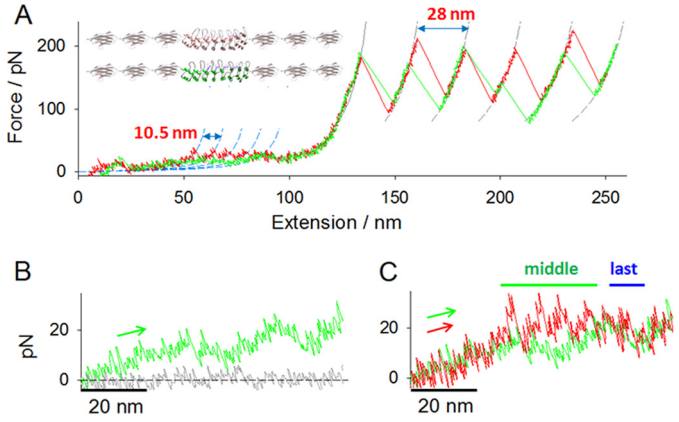

FIGURE 2. **Unfolding force-extension traces of WT NI6C and mutant NI(I_{H7R})$_4$IC.** *A*, schematic diagrams of NI6C-I27 and NI(I_{H7R})$_4$IC-I27 chimeric proteins (*inset*) and their representative unfolding traces at a pulling speed of 0.1 nm/ms. Force peaks of NI6C-I27 are fitted to two families of worm-like chain curves, with contour length increments (ΔL_c) of 10.5 nm (*blue dashed lines*; persistence length of ~0.7 nm) and 28 nm (*gray dashed lines*; persistence length of ~0.36 nm), corresponding to the unfolding of individual ARs (33 amino acids × 0.365 nm/amino acids − 0.8 nm (folded length)) and of I27 domains (89 amino acids × 0.365 nm/amino acids − 4 nm (folded length)), respectively. *B*, magnified portion of the unfolding force-extension curve of NI(I_{H7R})$_4$IC-I27 in *A* corresponding to the extension between 25 and 100 nm. The *gray trace* and the *black dashed line* show the force base line. *C*, comparison of the mutant force-extension trace (*green*; the same trace in *A*) with the WT unfolding force-extension trace (*red*; the same trace in *A* and *B*). The unfolding force peaks are divided into two groups: middle peaks (*green bar*) and last peaks (*blue bar*).

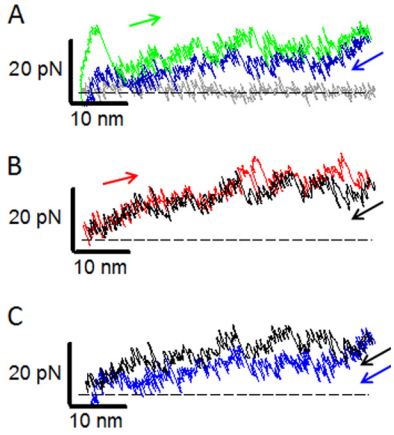

FIGURE 3. **Unfolding and refolding force-extension traces of WT NI6C and mutant NI(I_{H7R})$_4$IC.** *A*, set of unfolding (*green*) and refolding (*blue*) force-extension traces of NI(I_{H7R})$_4$IC. The *gray trace* and the *black dashed line* show the force base line. *B*, set of unfolding (*red*) and refolding (*black*) force-extension traces of NI6C. The *black dashed line* shows the force base line. *C*, comparison of the refolding traces of NI(I_{H7R})$_4$IC (*blue trace* in *A*) and NI6C (*black trace* in *B*).

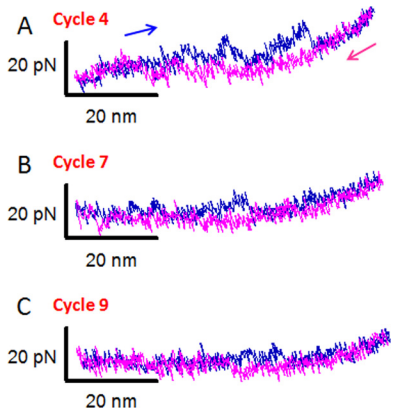

FIGURE 4. **Cyclic stretch-relax measurements of NI(I_{H7R})$_4$IC capture mechanical fatigue.** An NI(I_{H7R})$_4$IC molecule was partially stretched and relaxed at an extension rate of 0.03 nm/ms. After one stretch-relax measurement, the molecule was restretched after waiting 15~30 s.

the unfolding forces of the mutant are significantly lower compared with the unfolding forces of the WT protein. These observations are consistent with the design of the NI6C mutant, in which only the four internal repeats were mutated. We determined the mechanical energy consumed during the AR unfolding process by integrating the area between each force-extension curve and the worm-like chain curves (*yellow* area in supplemental Fig. S2, *C* and *D*). The average energy input necessary to mechanically unfold the mutant was 53.2 ± 10.9 kcal/mol (n = 50), and that for the WT protein was 106.5 ± 12.7 kcal/mol (n = 12). Thus, the four internal AR His → Arg mutations resulted in the ~53-kcal/mol decrease in the work necessary to unravel the mutated ARs compared with the WT ARs. In summary, the mechanical unfolding forces of the mutated ARs are significantly lower than those of the WT ARs. These observations confirm our expectations that the His → Arg mutations in TPLH motifs may reduce the mechanical stability of ARs.

Mechanical Refolding of NI(I_{H7R})$_4$IC in Cyclic Measurements—To examine the mechanical refolding behavior of NI(I_{H7R})$_4$IC, we performed cyclic stretch-relax measurements on the NI(I_{H7R})$_4$IC-I27 construct. During these measurements, the stretching distance was limited to unfold most of the ARs of the NI(I_{H7R})$_4$IC insert without unfolding of any of the I27 domains. Because the I27 domains remained folded, they did not interfere with the folding of ARs during the relaxation step. In Fig. 3*A*, a typical stretching force-extension curve of the mutant NI(I_{H7R})$_4$IC protein obtained under such partial unfolding conditions is superimposed with its refolding force-extension trace. In contrast to the large and sharp refolding force peaks of the WT NI6C protein (*black trace* in Fig. 3*B*) (7), the refolding force peaks of the mutant are smaller and somewhat smeared. The refolding traces of the WT and mutant proteins are superimposed in Fig. 3*C*. During repetitive stretch-relax measurements on the mutant, the refolding force peaks diminished, further indicating some refolding "fatigue" (Fig. 4 and supplemental Fig. S3, *A–C*) that was not observed for the WT protein (supplemental Fig. S3, *D–F*; see supplemental data in Ref. 7). In summary, His → Arg substitution in the TPLH motif seems to significantly affect the mechanical unfolding and refolding behavior of consensus ARs.

Our MD and AFM results revealed that His → Arg substitutions in TPLH motifs 1) eliminate inter-repeat H-bonds, greatly increasing the flexibility in the loop regions, which lessens the mechanical stability of the mutated ARs; 2) decrease the observed unfolding and refolding forces compared with those of the WT protein when both proteins are stretched by their termini (mechanical unfolding energy of 53 *versus* 106 kcal/mol); and 3) cause mechanical fatigue, which is absent in the WT protein. These results indicate that the mutated ARs in NI(I_{H7R})$_4$IC unfold easily and refold in a less springy, less robust manner compared with the WT protein. We hypothesize that the His → Arg mutation in ankyrin-R may cause HS by altering its tertiary structure and decreasing its mechanical robustness.

Repetitive deformations of ankyrin-R during circulation of RBCs may induce the HS mutant to progressively lose its structure and elastic properties, leading to the mechanical failure of ankyrin-R. This could in turn perturb the protein network mediated by ankyrin-R and disrupt important membrane-cytoskeleton connections.

Acknowledgments—We thank Jane Clarke for providing the plasmids with poly-I27 domains. Supercomputer time was provided by the Texas Advance Computing Center at The University of Texas at Austin as part of XSEDE (National Science Foundation Grant OCI-1053575), and the parallel computing resource was provided by the Computational Science and Engineering Program at the University of Illinois as part of the Taub cluster.

REFERENCES

1. Bennett, V., and Baines, A. J. (2001) Spectrin- and ankyrin-based pathways: metazoan inventions for integrating cells into tissues. *Physiol. Rev.* **81,** 1353–1392
2. Michaely, P., Tomchick, D. R., Machius, M., and Anderson, R. G. (2002) Crystal structure of a 12-ANK repeat stack from human ankyrin-R. *EMBO J.* **21,** 6387–6396
3. Ferreiro, D. U., Cho, S. S., Komives, E. A., and Wolynes, P. G. (2005) The energy landscape of modular repeat proteins: topology determines folding mechanism in the ankyrin family. *J. Mol. Biol.* **354,** 679–692
4. Lee, G., Abdi, K., Jiang, Y., Michaely, P., Bennett, V., and Marszalek, P. E. (2006) Nanospring behavior of ankyrin repeats. *Nature* **440,** 246–249
5. Li, L., Wetzel, S., Plückthun, A., and Fernandez, J. M. (2006) Stepwise unfolding of ankyrin repeats in a single protein revealed by atomic force microscopy. *Biophys. J.* **90,** L30–L32
6. Kim, M., Abdi, K., Lee, G., Rabbi, M., Lee, W., Yang, M., Schofield, C. J., Bennett, V., and Marszalek, P. E. (2010) Fast and forceful refolding of stretched α-helical solenoid proteins. *Biophys. J.* **98,** 3086–3092
7. Lee, W., Zeng, X., Zhou, H. X., Bennett, V., Yang, W., and Marszalek, P. E. (2010) Full reconstruction of a vectorial protein folding pathway by atomic force microscopy and molecular dynamics simulations. *J. Biol. Chem.* **285,** 38167–38172
8. Serquera, D., Lee, W., Settanni, G., Marszalek, P. E., Paci, E., and Itzhaki, L. S. (2010) Mechanical unfolding of an ankyrin repeat protein. *Biophys. J.* **98,** 1294–1301
9. Sotomayor, M., Corey, D. P., and Schulten, K. (2005) In search of the hair-cell gating spring elastic properties of ankyrin and cadherin repeats. *Structure* **13,** 669–682
10. Wetzel, S. K., Settanni, G., Kenig, M., Binz, H. K., and Plückthun, A. (2008) Folding and unfolding mechanism of highly stable full consensus ankyrin repeat proteins. *J. Mol. Biol.* **376,** 241–257
11. Guo, Y., Yuan, C., Tian, F., Huang, K., Weghorst, C. M., Tsai, M. D., and Li, J. (2010) Contributions of conserved TPLH tetrapeptides to the conformational stability of ankyrin repeat proteins. *J. Mol. Biol.* **399,** 168–181
12. Interlandi, G., Wetzel, S. K., Settanni, G., Plückthun, A., and Caflisch, A. (2008) Characterization and further stabilization of designed ankyrin repeat proteins by combining molecular dynamics simulations and experiments. *J. Mol. Biol.* **375,** 837–854
13. Binz, H. K., Stumpp, M. T., Forrer, P., Amstutz, P., and Plückthun, A. (2003) Designing repeat proteins: well expressed, soluble, and stable proteins from combinatorial libraries of consensus ankyrin repeat proteins. *J. Mol. Biol.* **332,** 489–503
14. Eber, S., and Lux, S. E. (2004) Hereditary spherocytosis: defects in proteins that connect the membrane skeleton to the lipid bilayer. *Semin. Hematol.* **41,** 118–141
15. Bennett, V., and Healy, J. (2008) Organizing the fluid membrane bilayer: diseases linked to spectrin and ankyrin. *Trends Mol. Med.* **14,** 28–36
16. Gallagher, P. G. (2005) Hematologically important mutations: ankyrin variants in hereditary spherocytosis. *Blood Cells Mol. Dis.* **35,** 345–347
17. Shrier, S. L., Rachmilewitz, E., and Mohandas, N. (1989) Cellular and membrane properties of α and β thalassemic erythrocytes are different: Implication for differences in clinical manifestations. *Blood* **74,** 2194–2202
18. Johnson, C. P., Tang, H. Y., Carag, C., Speicher, D. W., and Discher, D. E. (2007) Forced unfolding of proteins within cells. *Science* **317,** 663–666
19. Rief, M., Gautel, M., Oesterhelt, F., Fernandez, J. M., and Gaub, H. E. (1997) Reversible unfolding of individual titin immunoglobulin domains by AFM. *Science* **276,** 1109–1112
20. Oberhauser, A. F., Marszalek, P. E., Erickson, H. P., and Fernandez, J. M. (1998) The molecular elasticity of the extracellular matrix protein tenascin. *Nature* **393,** 181–185
21. Li, H., Linke, W. A., Oberhauser, A. F., Carrion-Vazquez, M., Kerkvliet, J. G., Lu, H., Marszalek, P. E., and Fernandez, J. M. (2002) Reverse engineering of the giant muscle protein titin. *Nature* **418,** 998–1002
22. Randles, L. G., Rounsevell, R. W., and Clarke, J. (2007) Spectrin domains lose cooperativity in forced unfolding. *Biophys. J.* **92,** 571–577
23. Brown, A. E., Litvinov, R. I., Discher, D. E., and Weisel, J. W. (2007) Forced unfolding of coiled coils in fibrinogen by single-molecule AFM. *Biophys. J.* **92,** L39-L41
24. Junker, J. P., Ziegler, F., and Rief, M. (2009) Ligand-dependent equilibrium fluctuations of single calmodulin molecules. *Science* **323,** 633–637
25. Puchner, E. M., and Gaub, H. E. (2009) Force and function: probing proteins with AFM-based force spectroscopy. *Curr. Opin. Struct. Biol.* **19,** 605–614
26. Lv, S., Dudek, D. M., Cao, Y., Balamurali, M. M., Gosline, J., and Li, H. (2010) Designed biomaterials to mimic the mechanical properties of muscles. *Nature* **465,** 69–73
27. Williams, P. M., Fowler, S. B., Best, R. B., Toca-Herrera, J. L., Scott, K. A., Steward, A., and Clarke, J. (2003) Hidden complexity in the mechanical properties of titin. *Nature* **422,** 446–449
28. Gao, M., Lu, H., and Schulten, K. (2001) Simulated refolding of stretched titin immunoglobulin domains. *Biophys. J.* **81,** 2268–2277
29. Best, R. B., Fowler, S. B., Herrera, J. L., Steward, A., Paci, E., and Clarke, J. (2003) Mechanical unfolding of a titin Ig domain: structure of transition state revealed by combining atomic force microscopy, protein engineering, and molecular dynamics simulations. *J. Mol. Biol.* **330,** 867–877
30. Sotomayor, M., and Schulten, K. (2007) Single-molecule experiments *in vitro* and *in silico*. *Science* **316,** 1144–1148
31. Li, M. S., Hu, C. K., Klimov, D. K., and Thirumalai, D. (2006) Multiple stepwise refolding of immunoglobulin domain I27 upon force quench depends on initial conditions. *Proc. Natl. Acad. Sci. U.S.A.* **103,** 93–98
32. Mickler, M., Dima, R. I., Dietz, H., Hyeon, C., Thirumalai, D., and Rief, M. (2007) Revealing the bifurcation in the unfolding pathways of GFP by using single-molecule experiments and simulations. *Proc. Natl. Acad. Sci. U.S.A.* **104,** 20268–20273
33. Makarov, D. E. (2009) A theoretical model for the mechanical unfolding of repeat proteins. *Biophys. J.* **96,** 2160–2167
34. Gao, M., Craig, D., Lequin, O., Campbell, I. D., Vogel, V., and Schulten, K. (2003) Structure and functional significance of mechanically unfolded fibronectin type III_1 intermediates. *Proc. Natl. Acad. Sci. U.S.A.* **100,** 14784–14789
35. Steward, A., Toca-Herrera, J. L., and Clarke, J. (2002) Versatile cloning system for construction of multimeric proteins for use in atomic force microscopy. *Protein Sci.* **11,** 2179–2183
36. Marszalek, P. E., Oberhauser, A. F., Pang, Y. P., and Fernandez, J. M. (1998) Polysaccharide elasticity governed by chair-boat transitions of the glucopyranose ring. *Nature* **396,** 661–664
37. Rabbi, M., and Marszalek, P. E. (2007) Measuring protein mechanics by atomic force microscopy. *Cold Spring Harbor Protoc.* **2007,** 10.1101/pdb.prot4901
38. Florin, E. L., Rief, M., Lehmann, H., Ludwig, M., Dornmair, C., Moy, V. T., and Gaub, H. E. (1995) Sensing specific molecular interactions with the atomic force microscope. *Biosens. Bioelectron.* **10,** 895–901
39. Humphrey, W., Dalke, A., and Schulten, K. (1996) VMD: Visual molecular dynamics. *J. Mol. Graph Model.* **14,** 33–38
40. Phillips, J. C., Braun, R., Wang, W., Gumbart, J., Tajkhorshid, E., Villa, E., Chipot, C., Skeel, R. D., Kalé, L., and Schulten, K. (2005) Scalable molecular dynamics with NAMD. *J. Comput. Chem.* **26,** 1781–1802
41. Lu, H., Isralewitz, B., Krammer, A., Vogel, V., and Schulten, K. (1998)

Unfolding of titin immunoglobin domains by steered molecular dynamics stimulation. *Biophys. J.* **75,** 662–671

42. Merz, T., Wetzel, S. K., Firbank, S., Plückthun, A., Grütter, M. G., and Mittl, P. R. (2008) Stabilizing ionic interactions in a full consensus ankyrin repeat protein. *J. Mol. Biol.* **376,** 232–240
43. MacKerell, A. D., Jr., Bashford, D., Bellot, M., Dunbrack, R. L., Jr., Evanseck, J. D., Field, M. J., Fischer, S., Gao, J., Guo, H., Ha, S., Joseph-McCarthy, D., Kuchnir, L., Kuczera, K., Lau, F. T., Mattos, C., Michnick, S., Ngo, T., Nguyen, D. T., Prodhom, B., Reiher, W. E., III, Roux, B., Schlenkrich, M., Smith, J. C., Stote, R., Straub, J., Watanabe, M., Wiórkiewicz-Kuczera, J., Yin, D., and Karplus, M. (1998) All-atom empirical potential for molecular modeling and dynamics studies of proteins. *J. Phys. Chem. B* **102,** 3586–3616
44. Perez-Jimenez, R., Garcia-Manyes, S., Ainavarapu, S. R., and Fernandez, J. M. (2006) Mechanical unfolding pathways of the enhanced yellow fluorescent protein revealed by single-molecule force spectroscopy. *J. Biol. Chem.* **281,** 40010–40014
45. Dietz, H., and Rief, M. (2004) Exploring the energy landscape of GFP by single-molecule mechanical experiments. *Proc. Natl. Acad. Sci. U.S.A.* **101,** 16192–16197
46. Word, J. M., Lovell, S. C., LaBean, T. H., Taylor, H. C., Zalis, M. E., Presley, B. K., Richardson, J. S., and Richardson, D. C. (1999) Visualizing and quantifying molecular goodness of fit: small probe contact dots with explicit hydrogen atoms. *J. Mol. Biol.* **285,** 1711–1733
47. Word, J. M., Lovell, S. C., Richardson, J. S., and Richardson, D. C. (1999) Asparagine and glutamine: using hydrogen atom contacts in the choice of side chain amide orientation. *J. Mol. Biol.* **285,** 1735–1747
48. Davis, I. W., Leaver-Fay, A., Chen, V. B., Block, J. N., Kapral, G. J., Wang, X., Murray, L. W., Arendall, W. B., 3rd, Snoeyink, J., Richardson, J. S., and Richardson, D. C. (2007) MolProbity: all-atom contacts and structure validation for proteins and nucleic acids. *Nucleic Acids Res.* **35,** W375–W383
49. Brooks, C. L., 3rd (2004) Extending the treatment of backbone energetics in protein force fields: Limitations of gas-phase quantum mechanics in reproducing protein conformational distributions in molecular dynamics stimulations. *J. Comput. Chem.* **25,** 1400–1415